

A Compact Radiometric Microwave Calibrator

D J Fixsen, SSAI Goddard Spaceflight Center Greenbelt MD 20771, E J Wollack²,
A Kogut Code 665 Goddard Spaceflight Center Greenbelt MD 2077, M Limon Code 665
Goddard Spaceflight Center Greenbelt MD 2077, P Mirel, SSAI Goddard Spaceflight
Center Greenbelt MD 2077, J Singal University of California, Santa Barbara and
S M Fixsen SSAI Goddard Spaceflight Center Greenbelt MD 2077

ABSTRACT

The calibration methods for the ARCADE II instrument are described and the accuracy estimated. The Steelcast coated aluminum cones which comprise the calibrator have a low reflection while maintaining 94% of the absorber volume within 5 mK of the base temperature (modeled). The calibrator demonstrates an absorber with the active part less than one wavelength thick and only marginally larger than the mouth of the largest horn and yet black (less than -40 dB or 0.01% reflection) over 5 octaves in frequency.

Subject headings: Radiometric Reference Loads; Cryogenic Instrumentation.

1. Introduction

We describe the performance of a blackbody calibrator for the Absolute Radiometer for Cosmology, Astrophysical and Diffuse Emission (ARCADE II) instrument. The primary goal of the ARCADE II experiment is to compare the Cosmic Microwave Background (CMB) spectrum to a blackbody spectrum at long wavelengths, where the first stars are predicted to distort the ideal blackbody spectrum of the Big Bang¹. The ARCADE II instrument has seven Dicke switched radiometers (Fig. 1), each with a corrugated horn antenna, internal calibrator, and amplifier, mounted in an open liquid helium dewar to measure the absolute brightness, or temperature, of the CMB from 3 to 90 GHz to 1 mK precision. The dewar is 1.5 m in diameter and 1.8 m deep to contain all seven radiometers (the largest of which is 620 mm in diameter at its mouth and ~ 1.5 m long) and 1-2 m³ of liquid helium to cool the apparatus to approximately the temperature of the CMB (2.7 K). The dewar top is capped with an aluminum aperture plate, which contains the apertures of all 7 radiometer corrugated horns. Just above the aperture plate is a second plate (the carousel; Fig. 2) that can

rotate. The carousel has two holes. One hole has a stainless steel flare around the edge but is otherwise open to the sky. The other hole is filled by the calibrator. The carousel rotates around the center of the dewar to three positions. The radiometers are organized into three groups. In each of the carousel positions, one group of radiometers observes the sky, a second group observes the calibrator and the third group is blocked by the carousel. By rotating the carousel to each of its three positions, all of the radiometers in turn can see the calibrator and the sky. To minimize the uncertainty from atmospheric emission the ARCADE II instrument is carried aloft with a high altitude balloon. A previous experiment, ARCADE I², demonstrated the feasibility of this type of measurement. The first ARCADE II flight was on July 28, 2005 on a 28 million cubic foot helium balloon to 35 km altitude from the National Scientific Balloon Facility (NSBF) in Palestine, TX.

ARCADE II employs a double difference scheme to control systematic errors, similar to the design of the COBE FIRAS instrument³. The input to each amplifier is switched at 75 Hz between an antenna and an internal calibrator⁴. The

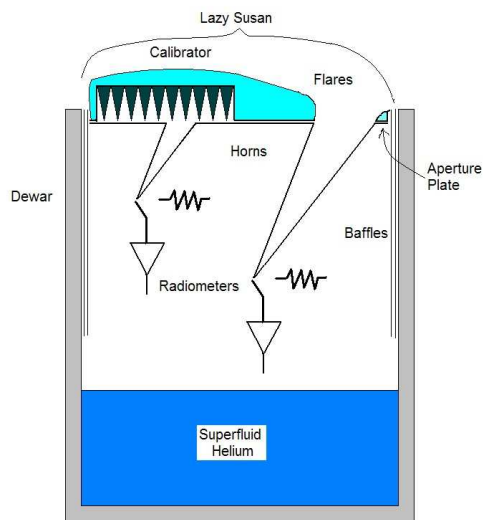


Fig. 1.— A cartoon of the ARCADE II instrument. The lazy susan pivots about the center of the dewar on the top, allowing all seven of the radiometers to be calibrated. Light enters the horn from the sky or the calibrator. A switch on each radiometer alternately couples the horn or the reference load to the amplifier. After amplification the signal is demodulated in the warm electronics. All 7 channels are similar.

temperature of the internal calibrator can be adjusted to match the input from the antenna to null the signal at the switch frequency. This effectively eliminates gain and noise temperature drifts of the amplifier as sources of error. The combination of radiometer and internal calibrator serves as a transfer standard. They need to be stable for only a few minutes to allow comparison of the external calibrator to the sky.

The carousel can be rotated over the antennas so that each antenna views either the sky or the external calibrator, providing a second level of differencing. The critical measurement is the temperature difference between the sky and the external calibrator. The external calibrator provides an absolute reference by replacing the sky signal with a source of known temperature while all of the other parts of the instrument remain in similar states. There are three



Fig. 2.— Two of the authors lower the lazy susan onto the ARCADE instrument. The calibrator cones are visible through the hole in the lazy susan at right. On the left is the hole with the flare for viewing the sky. At the bottom of the picture several conical feed horns are visible. Once mounted, the lazy susan rotates about its center to allow each radiometer a view of the sky or the external calibrator.

requirements for the external calibrator. 1) It must have a well defined, known temperature. 2) It must have low reflectivity, r , or high emissivity, e ($e = 1 - r$). 3) It must completely fill the radiometers' field of view (no leakage). In order to be realizable, the calibrator must be limited in size, weight, and cost. ARCADE II includes a 3.5 GHz radiometer, so a simple scaling of the FIRAS calibrator⁵ would result in a calibrator 1 m long with a mass of 200 kg, such a large calibrator would be impractical for a balloon-borne instrument.

2. Calibrator Material and Design

To minimize size and weight, the external calibrator was constructed from 295 absorbing cones, each 88 mm long and 35 mm in diameter (Fig. 3). The absorber is Steelcast⁶ (a mixture of 30% stainless steel powder, alumina powder, and epoxy; which, given the cone geometry, provides the absorption over the microwave band. Each cone has an aluminum core to provide a mounting surface and increase the thermal conductivity. Each completed cone weighs

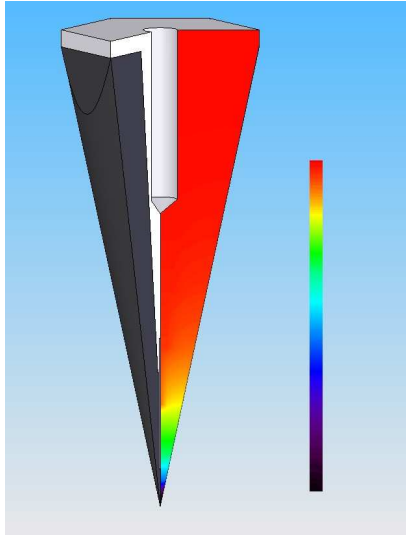


Fig. 3.— A cutaway view of a single cone. The half angle of the cone is 12° . The left side shows the internal structure. The light section is the aluminum core (a cone with a half angle of 6°). The hole at the top is threaded (1/4-20) to mount to the calibrator back plate. The dark section is Steelcast, the absorbing material of the calibrator. Note the copper wire extending from the aluminum cone into the tip section. The right side shows a thermal model of the calibrator cone. On the far right is a linear scale. The model suggests ~ 100 mK gradient from front to back, driven by the lower temperature aperture plane. Most of the gradient is very near the tip. 94% of the absorber volume is within 5 mK of the base temperature.

120 gm. The entire calibrator assembly, including a helium tank for cooling the calibrator, is an elliptical cylinder $600 \times 660 \times 150$ mm and weighs 55 kg. The temperature of the calibrator is measured by 26 thermometers embedded at various places in selected cones.

2.1. Thermal Design

The radiometers and aperture plate, including the horns, are cooled by boiling helium which at float altitude (~ 35 km) has a temperature of ~ 1.5 K. The lower parts of the instrument are surrounded by the dewar while the upper parts are protected from the tenuous atmosphere by ~ 5 m³/s of boiloff helium gas escaping from the

dewar.

Behind the back plate of the calibrator is a superfluid helium tank at ~ 1.5 K (Fig. 4). The superfluid helium is maintained by pumping helium from the reservoir in the dewar. The tank top as well as the rest of the carousel surface (except for the open hole to the sky) is covered with layers of aluminized mylar and styrofoam to minimize incoming radiation and stop any encroaching air. The helium tank provides additional shielding from radiation and air from above. The calibrator is weakly coupled to the superfluid helium tank through thermal standoffs. The calibrator temperature is controlled by heaters on the back of a diffuser plate.

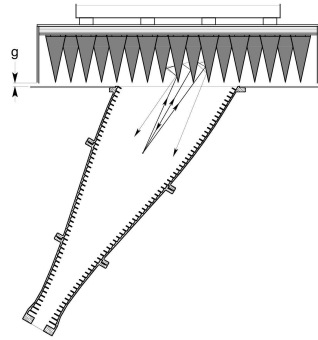


Fig. 4.— Schematic of calibrator in operation. In flight the gap labeled g is approximately 2 mm. In the test setup to measure the reflection of the calibrator it is varied over a quarter of a wavelength. A circular to rectangular transition is used to couple the input of the horn to waveguide. In flight the waveguide is attached to the switch. In the test, the waveguide is coupled to an HP8510C vector network analyzer to measure the reflection. Measurements were done at 3 to 90 GHz.

The aperture plane is cooled to ~ 1.5 K to minimize the radiation into the radiometers and to limit the heat load on the horns. The calibrator temperature is maintained at 2.7 K to mimic the sky. This introduces a thermal gradient between the aperture plane and the calibrator, which in turn sets up a thermal gradient within the calibrator.

To reduce the vertical thermal gradients, the core of each cone was made of aluminum to increase the thermal conductivity along the axis towards the tip. As long as the absorber is thicker than an electrical skin depth there is negligible radiometric penalty. At the tip of the cone where the radius of the cone is less than a skin depth, a copper wire was used to extend the thermal conductance along the axis. This is a compromise between the radiative properties and the thermal properties of the cone, but it is justified, as will be seen in the electromagnetic design section. The copper wire is bonded to the aluminum core with silver epoxy (Eccobond 83C/Cat9). A thermal model of the design is presented in Figure 3.

To reduce horizontal thermal gradients in the calibrator, the back of the calibrator consists of 50 alternating layers of 130 μm aluminum and 130 μm fiberglass sheets. This makes the diffuser plate have a modest vertical but high horizontal thermal conductivity. The edge of the calibrator is a double layer of aluminum. The outer layer blocks radiation or air and stops thermal conduction in the thin helium gas. The inner layer is a second line of defense that also forms a microwave cavity for the thermal radiation from the calibrator to the horn.

2.2. Thermal Gradient Model

The major thermal gradient is driven by the heat flow from the warm diffuser plate to the cooler aperture plane. Heat is conducted through the gaseous helium over the whole front surface of the calibrator. If heat is transported only by the thermal conductivity of stratified helium gas, the total power is about 250 mW. Radiation at these temperatures is insignificant, but the large flow rates of helium allow considerable uncertainty in the transport of heat by moving helium. To understand the thermal gradients in the calibrator, a finite element numerical model of the temperatures was made. The model used 3060 elements for a single cone with the boundary conditions of a uniform diffuser temperature one Kelvin warmer than the uniform aperture temperature. Since there are a large number of nearly identical cones no heat was allowed to flow horizontally. As seen in Figure 3, the thermal gradients are largely confined to the

tip. The copper wire reduces the gradient so that, in the model, 94% of the volume of the absorber is within 5 mK of the base temperature. At 2.8 K, Steelcast has a thermal conductivity of 0.02 W/m-K⁶, while aluminum has a conductivity of 70 W/m-K and copper has a conductivity of 200 W/m-K. Where there is aluminum or copper in the cones, it dominates the thermal conductivity. The boundary impedance between the aluminum and the Steelcast is not known but the adhesion between them is maintained over many thermal cycles in tests, so it probably adheres over a significant fraction of the surface. The heat capacity of the Steelcast is $C_p = 4$ mJ/gK at 2.8 K⁶, and its total mass is ~ 30 kg for all of the cones. The slowest measured time constant is ~ 20 sec at 2.8 K. This implies that the aluminum-to-Steelcast conductance is greater than 6 W/K and the effective thermal contact area is most of the surface of the aluminum cones.

2.3. Thermometry

The temperatures of various components of the ARCADE II instrument were monitored with RuO (ruthenium oxide)resistive thermometers⁷. The thermometers were measured using a square wave excitation current of 1.2 μA . The thermometers have separate current and voltage leads, so the lead resistances in the cryostat have little effect on the results. The excitation frequency was 75 Hz, low enough to minimize shunt capacitance effects. The input to each ohmmeter is multiplexed through a CMOS switch, so each ohmmeter can read 24 thermometers and 8 calibration resistors in every major frame of the telemetry (1.0667 sec). The ARCADE II instrument used five ohmmeters with a total of 120 thermometers to monitor the temperature distribution in the calibrator, the radiometers and critical components in the dewar.

The external calibrator was instrumented with 35 of these thermometers. Twenty-six thermometers were embedded in the steelcast absorber of 23 selected cones. The 26 thermometers were embedded at varying depths and radii to measure gradients from cone to cone within the calibrator as well as gradients within a typical cone. Three cones each had two thermometers. Since the

cones are nearly identical and reside in nearly identical environments the gradients within each cone should mimic the gradients measured in the instrumented cones. Since the gradients are predicted to be highest near the tips most of the thermometers are placed in positions near the tips. The remaining nine thermometers were applied on the back and sides of the calibrator and helium tank. As long as all of the significant gradients are sampled the detailed thermal performance of the calibrator can be determined after the observations.

The RuO thermometers temperature vs. resistance curves were calibrated after they were cast in the cones by cooling the cones along with a NIST calibrated RuO thermometer. The flight ohmmeters with a flight-like harness were used in the temperature-resistance calibration to include the shunt capacitance to first order. The self-heating power in the RuO thermistors is 0.6 nW at 2.7 K for the current since the thermometers are calibrated in situ any self heating is inherently included in the calibration. Since the thermometers are embedded in the absorber the self heating is negligible. At higher temperatures the heating is smaller and the thermal conductivity is larger, which further reduces the effect. The calibration uncertainty is less than 1 mK near 2.7 K rising to a few mK at 20 K. The calibration is augmented by observing the helium superfluid transition at 2.1768 K. These thermometers have demonstrated calibration stability to within 1 mK over four years⁸.

The calibrator temperature in flight was regulated by a digital servo loop that used two separate thermometers to control the heaters on the back of the diffuser plate. The servo loop is a PID (proportional, integral and differential) system that has separate adjustable gain parameters of $n = 0...255$ for the proportional, integral and differential gain. In principle the servo loop could be tuned to achieve critical damping. In practice, the system is operated in an overdamped configuration.

Systematic effects in the thermometers are important in determining the absolute temperature, and these are important in comparing the ARCADE II measurements with other measurements (eg. FIRAS). However, to

determine spectral distortions over the 3 to 90 GHz range it is only important to compare measurements across the ARCADE II radiometers. Since these share the same calibrator, systematic effects in the thermometry are eliminated to first order, leaving radiometric effects as the dominant residual systematic uncertainty.

2.4. Electromagnetic Design

The horn antennas are corrugated to have low side lobes⁹. They are tipped 30° from the vertical (Fig. 2) to avoid a direct view of the balloon and flight train. While observing the sky, the calibrator and other parts of the carousel are hidden by the flare which further reduces the side lobes. Ideally the calibrator mimics the response of the sky at all frequencies. Designing the calibrator for 5 octaves in frequency requires consideration of both the high frequency limit and the low frequency limit.

When the wavelength is large compared to the array periodicity, the technique of homogenization¹⁰ provides theoretical guidance for the calculation of the performance of the calibrator. In this limit the structure is effectively a one dimensional inhomogeneous anisotropic medium with propagation characteristics described by an effective dielectric parameter which varies as a function of length. This allows treatment of the problem as a one-dimensional transmission line with varying characteristic impedance and propagation constant. In the limit that the wavelength is small compared to all other characteristic length scales in the problem (the geometric limit) the calibrator can be treated by considering the reflection and absorption of the Steelcast using geometric optics.

Our design for the cone opening angle and dielectric layer thickness is guided by these considerations. A critical parameter is the thickness of the absorber layer. A thicker layer produces higher emissivity at the cost of larger thermal gradients. The Steelcast layer on the cone is 7 mm thick, the skin depth at the lowest frequency, to absorb the incident radiation before reflection from the underlying metal surface (Fig. 3). Electromagnetic simulations¹¹ validate the design assumptions and performance of the

calibrator for the nominal flight incidence angle, 30° , assuming a relative dielectric constant of $\epsilon_r \sim 10 + 2i$ for 30% Steelcast⁶. These simulations modeled an array of cones with periodic boundary conditions to represent an infinite calibrator structure with a rectangular lattice of cones. Once the basic cone geometry and electrical parameters were validated, the aluminum core employed to reduce the thermal gradient was modified until the predicted absorbance changed by a few percent. The key cone parameters are the sharpness of the cone tip and the dielectric loading of the absorber. The effective radius of the tips is roughly 0.3 mm.

We tested the model prediction using a WR-284 waveguide structure with both solid Steelcast and the final cone design^{12,13}. In these tests a pair of cones are placed at the end of a waveguide. The walls of the waveguide reflect the radiation, making the pair of cones at the end of the waveguide appear as an infinite grid of cones. These were measured with a network analyzer (Fig. 5). These waveguide tests validated the design geometry and electromagnetic models for a rectangular grid of cones. Measurements were made to determine the real and imaginary components of the dielectric constant at several frequencies at both room and cryogenic temperatures. These measurements show that the permeability is unity in the range of frequencies of interest.

2.5. Calibrator Reflectance Design

The calibrator is the dominant radiator in a cavity bounded by four surfaces: the calibrator, the corrugated horn⁹, the throat of the horn leading to the radiometer, and the gap between calibrator and horn. If the sky were a blackbody and all these surfaces were at the temperature of the sky, then the radiation inside the cavity would be perfect blackbody radiation and would have the same intensity and spectrum as the sky radiation. In that limit, moving the calibrator in or out of the beam would make no change in the radiation field. This is the basis for a precise differential comparison of the sky to the calibrator.

The leading deviations from the perfection of this blackbody cavity are as follows. First, there are small reflections at both ends of the horn and

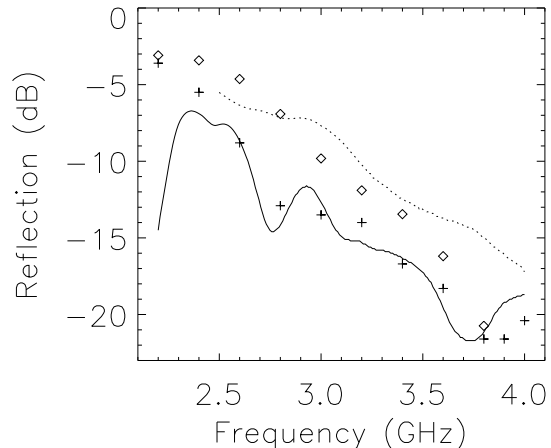


Fig. 5.— Results of models and measurements of the waveguide calibrator simulator. Reflections are for a calibrator simulator and not for the calibrator itself. Lines are measurements and the dots are calculations. The solid line is the measured data for solid dielectric cones with an aluminum backing; the corresponding modeled response ($\epsilon_r = 10 + 2i$) is indicated by the "+" symbols. The dotted line is the measured data for the dielectric cones with aluminum inner core and wire tip; the corresponding modeled response ($\epsilon_r = 10 + 2i$) is indicated by the diamonds. The cones comprising the calibrator are placed in a hexagonal close pack arrangement to increase the surface area and provide 5 ray bounces on average before the ray reenters the horn (Fig. 2). Modeling of the hexagonal pattern used in the calibrator predicts the reflection at 3 GHz to be less than -40 dB.

absorption in the horn. We absorb this term in the calibration gain constants of the radiometer model. Second, the horn is not at the same temperature as the sky or calibrator. We also include this term in the instrument model as the horn temperature is measured in flight. The leading term that is not included in the calibration model is the change in the emission of the instrument, at a temperature of about 1.5 K, that is induced by inserting the external calibrator. This term can not be included in the calibration model because the calibrator must be inserted to calibrate and must be out of the horn to view the sky. To first order, the error

introduced is

$$\delta T = r_i(T_i - T_c) \quad (1)$$

where δT is the error in emitted intensity, T_i and T_c are the instrument and calibrator temperatures, and r_i is the reflectivity of the calibrator for radiation originating in the instrument and reflected back toward it.

We estimate the specular reflectance of the calibrator by approximating it as an infinite array of hexagonal close packed cones. An ensemble of rays approximating the beam of the corrugated horn is tracked through the array of cones. The mean number of bounces before returning to the mouth of the horn is 5. For the all radiometers except the 3 GHz a significant fraction of the calibrator cones are blocked by the aluminum aperture plane. In this case the radiation reflects back into the calibrator, so the number of bounces is underestimated. We estimate the refractive index from the normal surface reflectance r_s and use the Fresnel formulas to compute all the reflectances. Averaging over polarizations, the predicted specular reflection is $r = -55$ dB at 30 GHz and 30° incidence angle. The absorber is not thick enough (7 mm) to be entirely opaque; attenuated 3 GHz radiation still reaches the aluminum cores. The half angle of the aluminum cores is steeper than the half angle of the Steelcast surface so this adds only a negligible fraction to the calculated specular reflection.

The diffuse reflection is governed by the surface texture, which is similar to that of a machined metal surface having a surface roughness of $\sigma \sim 5 \mu\text{m}$ rms. We approximate the calibrator diffuse reflectance by

$R_{\text{surf}} = 4R_n(\Omega/\pi) \sin(\psi/2)(\sigma k)^2$, where $k = 2\pi/\lambda$ is the wavevector, $R_n \approx 0.1$ is the normal reflectance of a polished surface, the solid angle not covered by some other part of the calibrator from the surface of a cone is $\Omega \sim \pi/2$, $\psi = 24^\circ$ is the full angle of the cone, and the sine function accounts for the angle of incidence of radiation from the radiometer. Although diffuse reflection is evident at visible wavelengths, evaluating at a wavelength of 3 mm, we find $R_{\text{surf}} = 4 \times 10^{-9}$, quite negligible, showing that a more exact calculation is unnecessary.

2.6. Gap Leakage

A clearance between the carousel and the aperture plate is required to allow the carousel to rotate in flight. The gap is similar in size (~ 2 mm or about .3% of the full 4π solid angle) for the flare (sky observation) and the calibrator. This gap is a potential radiation leak into the horn from a region of complicated geometry and temperature. Sources of warm radiation in flight include the multilayer insulation blanket on the outside of the calibrator and the top of the carousel. So a worst case calculation would introduce perhaps $40 \text{ K} \times .003 = 120 \text{ mK}$, but this is pessimistic because the gap is far from the main beam. At the longer wavelengths the gap is a small fraction of the wavelength and the horn is arranged so that it rejects the polarization of the gap leakage from the direction the horn is pointed. Of course many bounces within the calibrator can leave the leakage with any polarization, but the bounces also absorb most of the leakage. The gap is a larger fraction of a wavelength for shorter wavelengths, but for these antennas the gap is further away from the antenna aperture and much of the leakage is absorbed in the calibrator before it reaches the antenna.

Laboratory measurements of the gap leakage were made with the 3 and 90 GHz horns and calibrator in the flight configuration. A small antenna behind the gap was used to illuminate the gap. At 3 GHz the leakage was less than -43 db with the E field perpendicular to the gap and ~ -53 db with the E field parallel to the gap. At 90 GHz the leakage was less than -65 db for both polarizations, the limit set by the measurement noise floor.

3. Calibrator Measurements

The flight thermal situation is difficult to reproduce in the laboratory. The combination of a low radiation environment and low (~ 400 Pa) pressure, ambient air, and the generation of several cubic meters per second of helium gas from within the dewar make testing in a thermal-vacuum chamber impractical. This large helium flow would overwhelm available pumps. Actual flight of the instrument is the easiest way to test the thermal performance. The

radiometric properties of the calibrator were measured in a series of laboratory tests.

The calibrator reflection coefficient was measured in all six ARCADE bands with the calibrator and antennas in flight configuration. Additional measurements were made to characterize the reflection from cones with different absorber arrangements to validate the design prior to construction of the flight calibrator.

The reflectivity of the flight calibrator was measured in six bands from 2.6 to 118 GHz, corresponding to the ARCADE II channels. The measurements were performed with an HP8510C vector network analyzer followed by a rectangular to circular waveguide transition, and then the flight corrugated feed horns with 30° slice, viewing the calibrator as used in flight (Fig. 4). The system is calibrated in waveguide at the end of the rectangular waveguide with a TRL (thru-reflect-line) calibration.

To measure the performance of this quasi-optical calibrator we use a simple reflectometry technique to measure the return loss. The network analyzer is used to measure the reflection amplitude and phase across the frequency band. The reflection of the system is dominated by the reflections from the transition to the horn and the horn itself. To separate the interface reflection from the calibrator reflection, the measurement is repeated several times for various distances between calibrator and feed horn. As the calibrator is moved along its axis the phase of its residual reflections are changed, while the larger reflections from the other components of the test setup remain fixed. A least squares solution of

$$M(\nu) = H(\nu) + T(\nu)e^{2\pi i\nu z/u} \quad (2)$$

provides H and T , where $M(\nu)$ is the complex measured reflection, $H(\nu)$ is the complex reflection from the network analyzer interface with the antenna, $T(\nu)$ is the complex reflection from the calibrator, z is a measure of the distance between the horn and calibrator, ν is the frequency, and u is the phase velocity in the direction normal to the calibrator. This analysis implicitly assumes that the incident light does not leak around the calibrator, and that varying the spacing between the horn and the calibrator does not change the horn's reflectivity or the

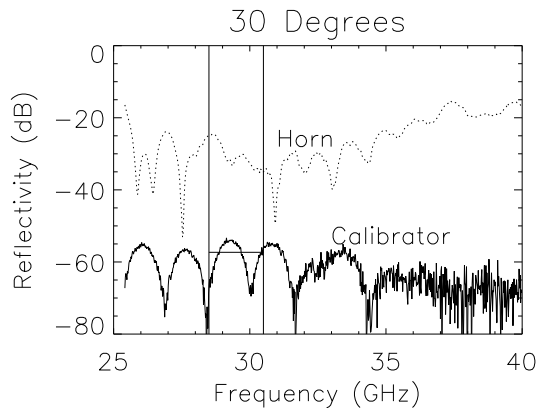


Fig. 6.— The least squares solution from four measurements of the reflection at 0, 125, 250 and 500 μm distance from the nominal position. The dotted line is the reflection of the test setup dominated by the reflection at the coax (not used in flight) to waveguide transition at the horn throat. The solid line shows the reflection of the calibrator. The vertical lines show the ARCADE II 30 GHz observing band.

network analyzer calibration. The validity of these assumptions is verified by inspection of the fit residuals for various configurations and by varying the details of the test set up.

The results of the 30 GHz measurement are shown in Figure 6. The noise floor appearing at ~ -70 dB is due to the limitations of the network analyzer calibration. The interference spectrum of the calibrator is consistent with the residual reflections from the cone tips and the point of cutoff near the cone bases. Similar measurements were performed at the other ARCADE frequencies.

The measured calibrator reflectivity for the ARCADE II bands are given in Table 1. We have also measured the calibrator reflectivity at normal incidence and note that it is only ~ 5 dB larger in magnitude than at the design angle. This is consistent with the anticipated performance given the variation in spike height and tip geometry across the calibrator section. We conclude that the calibrator is black ($r < -42$ dB) over the full five-octave range of the ARCADE II instrument.

This work was supported by the NASA Office of

Table 1: ARCADE II Calibrator Reflectivity Measurements

Waveguide	Band GHz	Reflected Power dB
WR284	3.4	-42.4
WR187	5.6	-55.5
WR112	8.3	-68.6
WR90	9.8	-62.7
WR28	30	-55.6
WR10	90	-56.6

Space Science under RTOP 188-02-54-01.

REFERENCES

- [1] Barlett, J.G. & Stebbins, A. 1991, ApJ, 371, 8
- [2] Kogut, A. et al. , 2004, ApJS, 154, 493
- [3] Fixsen, D.J. et al. , 1996, ApJ, 473, 576
- [4] Wollack, E.J. et al. , 2006, (Submitted)
- [5] Fixsen, D.J. et al. , 1999, ApJ, 512, 511
- [6] Wollack, E.J. et al. , 2006, RSI (Submitted)
- [7] Fixsen, D.J. et al. , 2002, RSI, 73, 3659
- [8] Kogut, A. et al. , 2004, RSI, 75 (12): 5079
- [9] Singal, J. et al. , 2005, RSI, 76, 124073
- [10] Kuester, E.F., Holloway, C.L., 1994,
Transactions on Electromagnetic
Compatibility, Vol. 36, No. 4, pp. 300-313.
- [11] Ansoft, HFSS (High Frequency Structure
Simulator), 225 West Station Square Drive
Suite 200, Pittsburgh, PA 15219.
- [12] R.C. Hansen, Phased Array Antennas, 1998,
John Wiley and Sons, New York, pp. 458.
- [13] Hannan, P.W., and Balfour, M.A., 1965,
IEEE Transactions on Antennas and
Propagation, Vol.13, No. 5, pp. 342-353.